DR2010170
Electronic supplementary materials to the Paper by Bindeman, Schmitt and Evans.

Samples

All ruby corundum-bearing samples (K1,2,3,5) come from two trenches that expose a single 300x40 m outcrop (locality 4, Fig.1) in the middle of the Khitostrov island with coordinates 66°N 20' (33''-37'') and 33°E 02' (20-23'') (Fig. A3-A4) while the corundum samples (K4,K6) come from the west of this outcrop near the shore (66°N 20'35'' 33°E02'20'') that embed the above corundum-bearing "matasomatites" bodies.

Analytical technique

Oxygen isotope analyses of plagioclase, rubies, kyanite, biotite, amphibole, garnet, zircon, monazite, and rutile relied on 0.5-2 mg aliquots and were performed at the University of Oregon stable isotope lab using CO_2-laser fluorination (Bindeman, 2008). We concentrated on single grain and core and rim parts of the same grain analyses where size permitted (shown in pink in Table 1). Small mineral grains of zircon, monazite and rutile were run as bulk and size fraction mixtures. Samples were heated up by a NewWave 35Watts laser in the presence of purified BrF_5 reagent to liberate oxygen. The gas generated in the laser chamber was purified through a series of cryogenic traps held at liquid nitrogen temperature, and a mercury diffusion pump to remove traces of fluorine gas. Oxygen was converted to CO_2 gas in a small platinum-graphite converter, the yields were measured, and then CO_2 gas was analyzed on a MAT 253 mass spectrometer in a dual inlet mode. Four to seven Gore Mt garnet standard ($\delta^{18}O$= 5.75‰) were analyzed together with the unknowns during each of seven analytical sessions. Day-to-day $\delta^{18}O$ variability of standards ranged from being 0.1 to 0.35‰ lighter than their reference values and the measurements of unknowns were adjusted to correct for day-to-day variability. The precision on standards is better than 0.1‰ 1 st dev on average.

Because samples were significantly lighter in $\delta^{18}O$ than our standard (and no standard as negative as the reported values exist to our knowledge), one might worry about analytical offsets related to the memory effects. However garnet standard run after –20‰ unknown did not display downward shift by more than –0.1‰ as compared to normal-$\delta^{18}O$ samples run in different data blocks of the same analytical session; we therefore accept that memory effects on the order of 0.1 ‰ could have affected the measured values but we choose not to apply any special corrections other then those outlined above, given the remarkably large $\delta^{18}O$ range found. Mass spectrometry analyses of isotopically negative samples vs a standard gas should not result in unexpected deltas because calculation of deltas is done using raw ratios.

We additionally performed oxygen isotope measurements for 2 samples using O_2 gas as analyte without converting it to CO_2 in order to check for mass-independent ^{17}O anomaly. This anomaly could signify potential extraterrestrial (e.g. cometary) origin of ultradepleted $\delta^{18}O$ Karelian gneisses, or Archean mass-independent effects due to atmospheric photolysis. The O_2 measurements are routinely performed at the University of Oregon Stable Isotope lab to characterize mass independent ^{17}O excesses in terrestrial (Martin and Bindeman 2009) and extraterrestrial materials such as HED meteorites (Ruzicka et al. in prep) and we have good calibration procedures for $\Delta^{17}O$. However two measurements yielded $\Delta^{17}O$ =0 permil thus denying the possibility of extraterrestrial or atmospheric photolytic origin.

Hydrogen isotope measurements relied on 1-2 mg of individual and bulk biotite and amphibole crystals and were performed in a continuous flow mode using UHP He carrier gas and TC/EA furnace with glassy carbon (improved after Sharp et al. 2001). We employed three out of four solid standards in three analytical sessions (NBS30 biotite, δD=-66‰, Water Canyon biotite, δD=-106‰, Butte Montana BUD biotite δD=–161.8‰, and RUH2 muscovite, δD=-98.2‰) spanning the range of 95‰ and overlapping with the ranges of the unknowns. We applied three point calibration using offsets between obtained δD values and the quoted values for mica standards run during each analytical session. Instrumental mass fractionation offset were typically between 20 and 30‰ and the magnitude of offset differed by less than 10‰ in

lighter vs. heavy D/H ends. Base on the repeat values of standards, the 1 st deviation ranged in the ±2-3‰ range. Furthermore, in the beginning of each analytical session we applied H3 factor at different pressure of the carrier gas to correct for different peak heights.Water concentrations were determined by mass H_2 peak integration and the uncertainty is estimated to be ±0.1wt% based on standards. As biotite and amphibole have ~4-4.5 and ~2 wt‰ H_2O respectively, the amount of alteration by chlorite (a phase with ~10wt% H_2O) can be estimated based on water concentration (high-H_2O samples, Table DR1b).

Whole-rock major and trace element concentrations were performed at the Washington State University by XRF and ICPMS methods (Table DR3, Fig. DR2).

Ion microprobe U-Pb dating of zircons and investigation of 18/16 ratio was performed at UCLA by Cameca 1270 large radius ion microprobe using standard procedures outlined in Schmitt et al. (2003) and Bindeman et al. (2006). Zircons were extracted from two crushed samples using standard density separation procedures involving heavy liquids and magnetic Franz separator. Extracted zircons were mounted in the conductive indium metal and polished to expose zircon cores. Dating included O2+ primary beam, initial presputtering and calibrations were performed using AS3 standard (Table DR2a).

Oxygen isotope analyses were performed after repolishing the indium mount down by ~10 microns (to remove pit topography and oxygen implanted during U-Pb dating analysis), used Cs primary beam, 25 micron beam size and targeted approximately the same spots as those used for dating. Relatively large beam size and repolishing likely resulted in core/rim overlap in some analyses. Measurements of two zircon standards (AS3, n=20, and KIM5, n=5) run before, during and after the unknowns, yielded IMF =2.91±0.08‰, and no $\delta^{18}O$ drift.

Monazite U-Th-Pb dating (Table DR2b) was performed on University of Oregon's Cameca SX100 electron microprobe using 300nA current, analytical and age derivation protocol from Montel et al. (1996).

Bindeman, I.N. 2008. Oxygen Isotopes in Mantle and Crustal Magmas as Revealed by Single Crystal Analysis. MINERALS, INCLUSIONS AND VOLCANIC PROCESSES, Reviews in Mineralogy and Geochemistry, Vol. 69, pp. 445-478.

Bindeman I.N., Schmitt A.K., Valley J.W. (2006) U-Pb zircon geochronology of silicic tuffs from the Timber Mt/Oasis Valley caldera complex, Nevada: rapid generation of large-volume magmas by shallow-level remelting. Contrib. Mineral. Petrol. 152:649-665.

Schmitt, A.K., Grove, M., Harrison, T.M., Lovera, O., Hulen, J.B., Walters, M., 2003. The Geysers–Cobb mountain magma system California (Part 1): U–Pb zircon ages of volcanic rocks conditions of zircon crystallization and magma residence times. Geochim. Cosmochim. Acta 67, 3423–3442.

Martin, E; Bindeman, I (2009) Mass-independent isotopic signatures of volcanic sulfate from three supereruption ash deposits in Lake Tecopa, California. Earth Planet Sci Lett. 282: 102-114.

Montel, JM; Foret, S; Veschambre, M, Nicollet C, Provost A.1996. Montel Electron microprobe dating of monazite. Chem. Geol. 131: 37-53.

Sharp, ZD; Atudorei, V; Durakiewicz, T. 2001. A rapid method for determination of hydrogen and oxygen isotope ratios from water and hydrous minerals. Chem. Geol. 178: 197-210.

Table DR1-a Oxygen isotope analyses of individual minerals (red) and bulk mineral separates (blue) in crystal clusters
K-1-3 means sample K1, cluster 3, see Fig. A4

	δ18O, VSMOW, ‰							
	Monazite	Plag	Garnet	Amph	Zircon	Ruby	Biotite	Kyanite	Rutile
Sample K-1 Corundum plagiogneiss									
K-1		-19.25	-23.47	-21.74		-23.76	-22.52		-23.45
K-1		-18.24	-23.44	-21.37		-24.40			
K-1						-24.44			
K-1						-24.12			
K-1						-24.42			
K-1-1		-19.65				-24.30	-18.25		
K-1-2		-20.90				-24.04	-16.85		
K-1-3		-19.24				-24.16	-17.11		
K-1-4		-20.96				-24.21	-18.29		
K-1-5		-20.69				-22.13	rim of big		
Sample K-2 Corundum plagiogneiss									
K-2-1		-21.02	-22.44			-25.79	-21.65		
K-2-2						-26.32			
K-2-3		-23.45				-25.89			
K-2-4		-20.92	-24.65			-26.14	-23.57		
K-2-4				-24.84		-24.84			
Sample K-3 Corundum plagiogneiss						rim big			
K-3-1		-21.47		-25.52		-25.63	-25.04		-26.97
K-3-1						-24.29	core of big		
K-3-1						-23.62	rim of big		
K-3-1						-23.47	core of big		
K-3-2		-19.74				-22.84			
K-3-2						-23.85			
K-3-3		-22.50				-26.07			
K-3-5						-25.79	-16.67		
Sample K-4 Kyanite-Corundum plagiogneiss, melanocratic									
K-4		-15.28				-17.74	-18.06	-19.97	-21.87
K-4-2	-17.45	-14.76				-18.51	-18.09		
K-4-2						-18.09			
K-4-3		-15.76				-18.44	-17.89	-19.83	
K-4-3							-17.53		
K-4-4		-14.75				-18.127	-18.10	-20.01	
								-18.09	
Sample K-5 Corundum plagiogneiss									
K-5		-20.05	-23.23	-22.88	-17.97	-23.06			-27.9
K-5		-19.75	-22.90	-22.56	-19.85	-22.74			
K-5		-20.44			-15.00				
Sample K-6 Kyanite-Corundum plagiogneiss, leucocratic									
K-6		-17.33				-18.57	-19.62	-19.96	-20.35
K-6								-20.00	
								-20.59	

Sample K-3 run as O2 gas

		δ18O, ‰	d17O	Δ17O = 1000*Ln[(δ17O/1000)+1] - 0.5259*1000*Ln[(δ18O/1000)+1]
K-3	Ruby-1	-27.04	-14.36	-0.05 ±0.036
K-3	Plag-1	-20.63	-10.96	-0.06 ±0.037

Table DR1-b
Hydrogen Isotope analyses of biotite, amphibole, and alteration minerals

		wt% H2O	dD
K-1	Amph	2.26	-159.1
K-1	Amph	2.36	-155.1
K-1	Amph	2.4	-143.5
K-1	Amph	1.8	-156.6
K-1	Biotite-1	4.93	-117.5
K-1	Biotite-1	4.62	-128.0
K-1	Biotite-1	4.01	-83.4
K-1	Biotite	4.1	-147.7
K-1	Biotite	4.8	-128.2
K-1	Biotite	3.6	-90.1
K-2	chlorite	10.6	-56.2
K-2	chlorite	11.6	-54.9
K-2-2	Biotite	3.9	-85.1
K-2-2	Biotite	3.8	-93.3
K-2-1	Biotite	4.3	-100.6
K-2-4	Biotite	3.3	-104.5
K-2-4	Amph	2.5	-139.8
K-3	Amph	3.0	-166.3
K-3-1	Amph	3.1	-132.0
K-3	Biotite	5.6	-110.0
K-3	Biotite	6.1	-93.4
K-3	Biotite	5.9	-88.5
K-3	Biotite-1	4.6	-188.9
K-3	Amph-1	2.6	-159.0
K-4	Biotite	3.7	-131.9
K-4	Biotite	3.7	-133.6
K-4-2	Biotite	3.7	-128.6
K-4-2	Biotite	3.7	-128.9
K-4-3	Biotite	3.7	-138.5
K-5	Amph	2.7	-142.2
K-5	Amph	2.8	-133.1
K-5	Amph	2.4	-144.9
K-6	Biotite	3.7	-131.0
K-6	Biotite	3.7	-129.7

Table DR2a: Sample K-5 U-Pb zircon geochronology and Oxygen Isotope analysis by ion microprobe

zircon	spot	comment	d18O	±1 s	206Pb*/ 238U	206Pb*/ 238U	207Pb*/ 235U	207Pb*/ 235U	207Pb*/ 206Pb*	Correlation 207Pb*/ 206Pb*	Age (Ma) of Concordia Ellipses	Age (Ma) 206Pb/ 238U	Age (Ma) 206Pb/ 238U	Age (Ma) 207Pb/ 235U	Age (Ma) 207Pb/ 235U	Age (Ma) 207Pb/ 206Pb	% Radiogen 207Pb/ 206Pb	Th/ 206Pb	Th/ U	1st	U	Th
				1 s.dev.*		1 s.e.		1 s.e.		1 s.e.			1 s.e.		1 s.e.		1 s.e.			1 s.e.	ppm	ppm
1	1	rim	-24.8	0.37	0.3573	0.0119	5.492	0.197	0.1115	0.0010	0.970	1969	57	1899	31	1824	16	99.6	0.027	0.0014	470	12.6
1	2	core	-25.1	0.37	0.3431	0.0096	5.337	0.154	0.1128	0.0010	0.954	1901	46	1875	25	1846	16	99.7	0.013	0.0009	380	4.8
1	3	core	-26.2	0.37	0.3186	0.0113	4.929	0.172	0.1122	0.0010	0.967	1783	55	1807	29	1836	16	99.4	0.026	0.0015	390	10.1
10	1	rim	3.0	0.37	0.4097	0.0096	9.068	0.222	0.1605	0.0010	0.969	2213	44	2345	22	2461	10	99.6	0.034	0.0011	920	31.2
10	2	core	7.3	0.37	0.5197	0.0162	12.86	0.41	0.1794	0.0006	0.995	2698	69	2669	30	2648	5	99.9	0.006	0.0004	1,350	7.4
11	1	core	6.4	0.37	0.5218	0.0202	12.71	0.50	0.1766	0.0007	0.995	2707	86	2658	37	2621	6	99.7	0.006	0.0006	940	5.2
11	2	rim	7.8	0.37	0.4884	0.0130	12.01	0.32	0.1783	0.0008	0.987	2564	57	2605	25	2637	7	99.7	0.005	0.0003	1,050	5.2
12	1	core	-26.1	0.37	0.3837	0.0119	6.751	0.231	0.1276	0.0013	0.956	2093	56	2079	30	2065	18	99.4	0.019	0.0009	460	8.6
12	2	rim	-16.9	0.37	0.3266	0.0100	5.151	0.181	0.1144	0.0017	0.908	1822	49	1845	30	1870	27	98.6	0.047	0.0018	410	19.2
13	1	core	4.9	0.37	0.4803	0.0156	11.25	0.35	0.1698	0.0008	0.990	2529	68	2544	29	2556	8	99.7	0.006	0.0005	900	5.0
14	1	rim	3.3	0.37	0.3249	0.0092	5.004	0.153	0.1117	0.0011	0.945	1814	45	1820	26	1827	18	99.4	0.142	0.0025	530	75.2
15	1	core	5.2	0.37	0.4240	0.0150	8.817	0.297	0.1508	0.0011	0.980	2278	68	2319	31	2355	12	99.6	0.039	0.0017	550	21.2
2	1	core	7.1	0.37	0.5133	0.0162	13.15	0.46	0.1858	0.0014	0.980	2671	69	2690	33	2705	12	99.8	0.016	0.0009	660	10.8
2	2	rim	5.4	0.37	0.4695	0.0160	10.98	0.38	0.1696	0.0006	0.995	2481	70	2521	33	2554	6	99.8	0.015	0.0011	670	10.2
3	1	rim	7.1	0.37	0.4821	0.0136	11.53	0.34	0.1735	0.0007	0.990	2536	59	2567	27	2592	7	99.8	0.005	0.0003	850	4.5
3	2	core	5.8	0.37	0.4880	0.0153	11.62	0.37	0.1726	0.0008	0.988	2562	66	2574	30	2583	8	99.8	0.017	0.0010	480	8.0
3	3	rim	5.8	0.37	0.5131	0.0150	12.91	0.38	0.1825	0.0005	0.996	2670	64	2673	28	2676	4	99.9	0.052	0.0012	1,580	81.8
4	1	rim	1.7	0.37	0.3494	0.0117	5.428	0.181	0.1127	0.0014	0.930	1932	56	1889	29	1843	23	99.0	0.017	0.0013	340	5.9
4	2	rim	-2.9	0.37	0.5305	0.0158	13.50	0.41	0.1846	0.0007	0.993	2744	66	2716	29	2695	6	99.9	0.155	0.0015	1,100	170.0
4	3	core	4.9	0.37	0.4618	0.0143	10.81	0.35	0.1698	0.0006	0.993	2447	63	2507	30	2556	6	99.6	0.019	0.0008	1,040	19.7
5	1	core	5.1	0.37	0.5049	0.0168	11.82	0.40	0.1698	0.0009	0.988	2635	72	2590	32	2556	9	99.7	0.057	0.0033	780	44.7
5	2	rim	7.0	0.37	0.4875	0.0295	11.08	0.71	0.1649	0.0029	0.962	2560	128	2530	60	2506	30	99.0	0.088	0.0033	630	55.6
6	1	rim	6.6	0.37	0.4443	0.0126	10.95	0.32	0.1787	0.0005	0.996	2370	56	2519	27	2641	4	99.6	0.024	0.0009	1,060	25.4
6	2	core	4.6	0.37	0.4478	0.0129	11.03	0.32	0.1787	0.0007	0.991	2385	57	2526	27	2641	6	99.6	0.019	0.0010	900	16.8
6	3	rim	3.7	0.37	0.4420	0.0133	10.86	0.34	0.1782	0.0010	0.986	2360	59	2511	29	2636	9	99.8	0.009	0.0004	1,110	10.4
7	1	rim	-24.1	0.37	0.3458	0.0097	5.335	0.166	0.1119	0.0010	0.964	1914	47	1875	27	1831	15	99.6	0.011	0.0009	450	5.1
7	2	core	-23.9	0.37	0.3486	0.0121	5.327	0.186	0.1108	0.0007	0.981	1928	58	1873	30	1813	12	99.5	0.008	0.0006	460	3.5
7	3	rim	-24.4	0.37	0.3201	0.0098	4.972	0.162	0.1127	0.0012	0.944	1790	48	1815	28	1843	19	99.5	0.017	0.0011	460	7.8
8	1	core	6.1	0.37	0.4560	0.0131	10.69	0.32	0.1700	0.0011	0.978	2422	58	2496	28	2557	11	99.8	0.006	0.0005	630	3.6
8	2	rim	6.5	0.37	0.4726	0.0158	10.75	0.37	0.1650	0.0013	0.971	2495	69	2502	32	2507	14	99.7	0.007	0.0008	510	3.4
9	1	rim	4.7	0.37	0.4665	0.0141	11.31	0.36	0.1758	0.0006	0.994	2468	62	2549	30	2613	6	99.7	0.088	0.0026	730	64.4
9	2	rim	5.7	0.37	0.5131	0.0135	12.67	0.34	0.1791	0.0015	0.952	2670	58	2656	26	2645	14	99.8	0.077	0.0015	1,010	77.5
9	3	core	6.3	0.37	0.4976	0.0138	12.31	0.35	0.1794	0.0007	0.991	2603	60	2628	26	2648	6	99.8	0.071	0.0015	970	69.0

* 1 st dev is based on measurements of two zircon standards (AS3, n=20, and KIM5, n=5) run before, during and after the unknowns, IMF =2.91±0.08‰ , no d18O drift was observed

Zircon 4

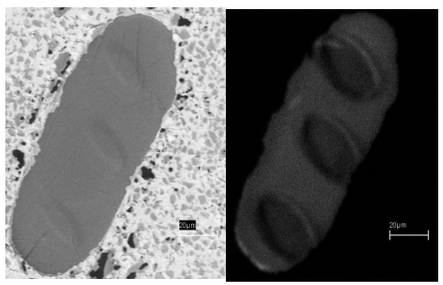

Zircon 14

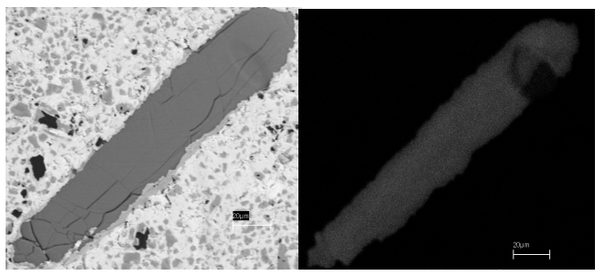

Zircon 12

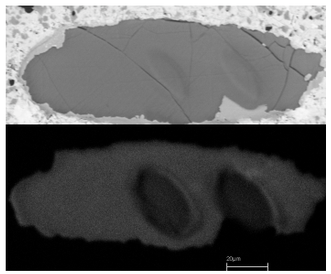

BSE and CL images of selected zircons pressed in indium mount

Table DR2b Sample K-4 Monazite geochronology determined by the electron microprobe

	Pb			Th			U			Montel		
Line nun	Conc (pp	% fit err.	LOD (ppm	Conc (ppm)	% fit err.	LOD (ppm)	Conc (ppm)	% fit err.	LOD (ppm)	Age	+	-
245	4718	2.24842	181.7	36435.0	0.631682	243.8	4360.3	1.59602	125.85	1923.6	54.3	54.3
246	4019	2.60654	185.3	31703.6	0.688575	242.1	4211.6	1.64099	125.45	1831.9	60.2	59.3
247	4116	2.54969	184.8	30954.8	0.70157	245.1	4019.4	1.71319	125.87	1925.4	62.6	61.6
248	4428	2.37979	182.8	33952.7	0.659599	242.7	4216.1	1.62727	124.19	1916.9	58.4	57.5
249	4018	2.58612	183.2	31943.7	0.687226	244.6	4083.7	1.68918	125.83	1840.7	58.5	58.5
250	4350	2.42429	183.8	34303.9	0.654733	241.9	4146.3	1.66248	125.38	1883.3	58.3	57.4
251	3799	2.71624	183.6	28281.7	0.744137	245.4	4218.8	1.63701	125.29	1862.7	64.0	62.9
252	4469	2.36409	183.2	36359.2	0.6327	244.2	4416.8	1.55955	123.8	1828.2	54.8	54.0
253	4643	2.27988	181.9	35808.7	0.638687	244.0	4327.9	1.60457	125.69	1921.5	56.4	55.5
254	4971	2.16477	183.2	39849.4	0.598195	245.4	4267.7	1.62758	126.08	1917.0	53.6	52.9
255	4523	2.34366	183.5	37185.8	0.625466	246.8	4505.4	1.54782	125.47	1812.0	53.6	51.6
256	4417	2.37841	182.1	32975.4	0.671874	242.7	3964.9	1.71909	124.49	1980.4	60.7	57.5
257	4879	2.21784	185.8	38663.8	0.609442	245.2	4180.6	1.65317	125.7	1932.4	55.3	54.5
258	5018	2.14001	182.1	38729.3	0.606696	241.8	4180.1	1.64883	125.24	1980.1	52.5	54.3
259	4657	2.31163	186.5	39330.0	0.602017	243.6	4134.5	1.66966	125.76	1836.7	54.0	53.3
260	4660	2.28	182.8	37738.7	0.618291	244.5	3983.6	1.7249	125.79	1905.8	55.9	55.1
261	4534	2.32332	181.7	36092.2	0.637056	246.4	3832.4	1.77703	125.11	1934.3	55.8	57.4
262	5124	2.10655	182.6	38309.7	0.610926	241.9	4849.3	1.45363	125.53	1950.9	53.0	52.4
263	5639	1.95121	183.0	44063.9	0.561897	244.6	5319.8	1.36321	128.19	1899.9	47.8	47.2
264	5644	1.94764	182.6	45389.0	0.552742	246.7	5387.9	1.33274	126.02	1859.3	46.4	45.8
265	6052	1.83481	181.6	47841.1	0.534181	244.0	5327.1	1.34879	126.47	1922.7	43.4	45.2
266	5937	1.86281	181.5	46120.3	0.545963	243.6	5584.0	1.29177	125.81	1909.0	43.5	45.3
267	5670	1.93605	182.0	44979.8	0.554281	243.5	5491.9	1.31378	126.36	1867.7	46.3	45.7
268	6704	1.70012	183.2	51281.2	0.512877	245.6	6665.4	1.12524	127.56	1895.7	41.4	40.9
269	4717	2.2535	182.4	39317.5	0.603635	246.2	3941.9	1.74894	126.61	1881.7	54.8	54.0
270	3934	2.63611	183.6	29683.9	0.718102	242.2	4305.5	1.60926	125.47	1856.0	61.5	60.6
271	4030	2.58119	183.5	33589.8	0.665132	244.4	3186.8	2.08744	124.82	1906.3	63.4	62.3
272	4148	2.52484	184.0	35158.5	0.648007	246.7	2926.4	2.24844	124.5	1934.8	61.4	62.6
273	3641	2.83705	185.5	34746.6	0.650638	243.5	3037.6	2.15959	123.43	1716.4	57.1	60.2
274	4003	2.6019	184.0	36667.2	0.631369	247.1	2784.0	2.34129	123.83	1836.1	61.5	60.5
275	3526	2.91373	185.2	34047.0	0.659601	244.0	2816.0	2.30987	123.32	1718.7	62.9	61.8
276	4471	2.3468	181.3	34858.2	0.648444	242.5	3834.2	1.77012	124.57	1948.6	61.5	53.8
277	4489	2.34692	182.3	36460.5	0.630563	243.0	3981.0	1.72068	125.35	1884.9	56.9	56.0
278	4774	2.23415	182.8	37802.5	0.61782	245.1	4498.0	1.55821	126.5	1884.4	53.9	53.2
279	5901	1.89779	185.7	45596.0	0.550043	244.5	5957.7	1.23499	127.63	1875.5	45.3	44.9
280	4656	2.26288	180.5	33885.9	0.66036	243.0	4495.1	1.54628	125.05	1970.0	57.3	56.5
281	4500	2.35268	183.5	36349.7	0.632942	244.8	4083.8	1.67881	124.94	1879.7	56.6	55.7
282	4662	2.27177	181.9	35945.7	0.638055	245.7	4199.0	1.64134	125.21	1941.1	54.4	56.2
283	4133	2.51432	182.1	32191.8	0.681881	242.4	4182.7	1.63729	124.2	1865.3	59.5	58.6
284	4512	2.34526	183.3	35313.3	0.643475	243.2	4216.2	1.63999	125.69	1902.9	57.2	56.3
285	4459	2.38403	185.0	35031.0	0.648287	245.3	4274.6	1.62048	125.67	1884.2	57.2	56.3
286	4699	2.27219	183.8	34635.4	0.65123	242.9	4332.9	1.5951	124.98	1982.7	55.2	57.3
287	4476	2.3697	184.3	33860.6	0.661308	244.1	4420.4	1.56823	125.03	1912.5	57.8	57.0
288	4126	2.52795	183.2	30374.2	0.707313	242.0	4204.4	1.63511	124.75	1925.3	61.9	60.9
289	4284	2.45675	184.1	3003.2	0.715861	246.2	4430.6	1.55621	124.05	1799.5	23.0	22.8

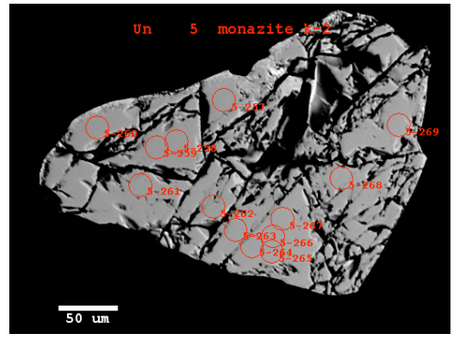

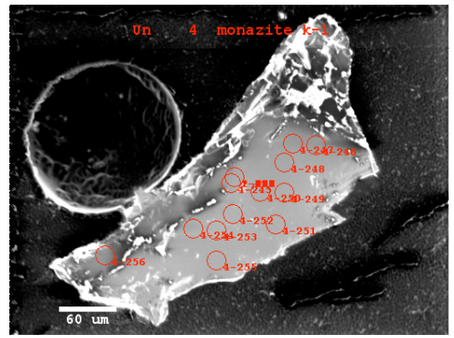

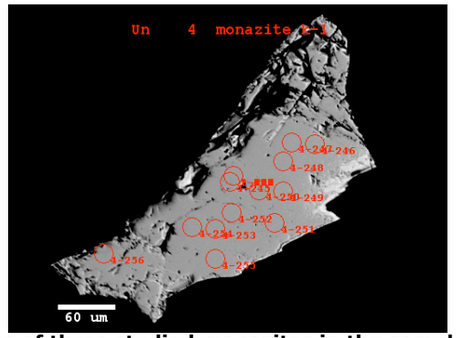

BSE Images of three studied monazites in the sample K-4

Table DR3 XRF and ICP MS analyses of studied rocks

XRF analyses

	K-1	K-2	K-4	K-6
Unnormalized Major Elements (Weight %):				
SiO2	53,09	55,13	44,75	59,99
TiO2	1,019	0,740	1,451	0,268
Al2O3	23,84	23,10	21,87	23,91
FeO*	5,01	4,34	11,98	1,56
MnO	0,040	0,020	0,096	0,008
MgO	3,67	3,82	7,97	1,24
CaO	4,49	4,32	1,60	3,94
Na2O	6,37	6,79	3,04	7,99
K2O	0,43	0,66	5,20	0,87
P2O5	0,041	0,028	0,020	0,112
Sum	98,01	98,95	97,99	99,88
Normalized Major Elements (Weight %):				
SiO2	54,17	55,71	45,67	60,06
TiO2	1,040	0,748	1,481	0,268
Al2O3	24,33	23,34	22,32	23,94
FeO*	5,11	4,39	12,23	1,56
MnO	0,041	0,021	0,098	0,008
MgO	3,75	3,86	8,14	1,24
CaO	4,58	4,37	1,63	3,95
Na2O	6,50	6,87	3,10	8,00
K2O	0,44	0,67	5,31	0,87
P2O5	0,042	0,028	0,021	0,112
Total	100,00	100,00	100,00	100,00
Norm. Corundum	4,94	3,44	8,55	2,93
Ni	167	188	341	56
Cr	324	281	472	131
Sc	17	18	47	4
V	167	136	285	60
Ba	94	207	1962	348
Rb	9	19	250	38
Sr	482	501	186	495
Zr	218	161	222	84
Y	18	12	24	3
Nb	10,9	6,9	6,5	2,9
Ga	34	30	45	30
Cu	4	0	4	1
Zn	37	20	162	24
Pb	13	15	10	16
La	47	45	18	15
Ce	115	103	42	29
Th	17	15	4	3
Nd	49	33	20	12
U	0	2	0	2
Cs	1	5	9	2

ICP-MS analyses

	K-1	K-2	K-4	K-6
Cs	0,39	0,71	7,58	1,17
Rb	8,3	18,0	239,1	36,4
Ba	90	198	1887	339
Th	17,45	15,78	4,60	3,01
U	1,64	1,21	0,98	0,68
Nb	10,45	6,34	5,99	2,26
Ta	0,68	0,38	0,45	0,15
K	3560	5514	43163	7187
La	55,40	50,03	16,34	12,66
Ce	116,14	98,84	34,57	26,29
Pb	10,52	14,35	8,45	14,64
Pr	13,81	10,86	4,12	3,20
Sr	476	493	183	480
Nd	50,44	36,31	15,98	12,71
Sm	9,48	4,95	3,30	2,89
Zr	216	159	220	83
Hf	5,98	4,33	6,11	2,32
Eu	1,56	1,27	0,79	1,52
Ti	6238	4487	8885	1607
Gd	6,43	2,89	3,34	2,10
Tb	0,76	0,37	0,62	0,18
Dy	4,00	2,16	4,22	0,63
Li				
Y	16,64	11,01	23,54	2,33
Ho	0,67	0,45	0,92	0,09
Er	1,58	1,19	2,61	0,21
Tm	0,22	0,17	0,40	0,03
Yb	1,33	1,06	2,47	0,17
Lu	0,21	0,17	0,42	0,03
Sc	19,6	18,6	48,9	4,4

Fig. DR1. Hydrogen and oxygen isotope analyses of biotite and amphibole crystals extracted from crystal clusters (see Tables DR1a and b for analyses). The range of δD and $\delta^{18}O$ values is interpreted here to indicate retrogressive exchange of initially ultra-low (ca –24 to –30‰ $\delta^{18}O$, -170 to -250‰ δD) protoliths with a variety of higher $\delta^{18}O$ and δD waters.

Amphiboles collectively have lower δD values (down to –167‰, Table DR1b) than biotites, maintain equilibrium $\Delta^{18}O$ fractionations (Fig. 1) and appear less retrogressed and retained greater proportion of the initial Paleoproterozoic ultra-depleted hydrogen. The lowest $\delta^{18}O$ and δD hydrous minerals would support a –28 to –30‰ $\delta^{18}O$ protolith. Yellow field and black dashed line represent inferred primary isotopic ranges of hydrous minerals in the protolith based on $\delta^{18}O$ range in refractory rubies parallel to the meteoric water line in different crystal clusters. The δD values in the primary protolithic micas and amphiboles were offset by -30‰ δD for water-mineral fractionation at metamorphic temperature of 600±100°C that correspond to metamorphic grade; at lower, ca 400°C temperature, the offset will be –50‰. Biotites that are most altered display higher water% (Table A1b) due to the presence of higher δD, higher H_2O chlorite; However, the lowest -189‰ Biotite in sample K-3 appears unaltered.

A retrogressive exchange at high temperatures (more than 300-400°C) is required to explain the isotopic trends and ranges. At low temperatures, hydration and alteration would yield perpendicular trend due to large positive $\Delta^{18}O$(mineral-water). Processes of metamorphic water loss and Rayleigh distillation via devolatilization would also produce more shallow negative slope on this diagram, contrary to the trend observed. Isotopic trends are curved concave up because water contain greater molar proportion of hydrogen than rocks. If modern-day meteoric water is taken as altering fluid, hydrous minerals record 4 to 20% retrogressive exchange, see 1-2% tickmarks on each mixing curve; if seawater ($\delta^{18}O$, δD = 0‰) is taken as altering fluid, then 1 to 5% fluid would suffice. Interaction with primary magmatic water ($\delta^{18}O$ and δD= -60±20‰, $\delta^{18}O$ = -5 to –8‰, e.g. Taylor and Sheppard, 1986) would require 2 to 8% of exchange. Deep magmatic, "metasomatizing" waters have been proposed to widely influence rocks from the Belomorian belt causing formation of metasomatites and pegmatites similar to those in Khitostrov (Terekhov, 2007; Ulyanov et al. 2008, Visotskii et al. 2008).

This diagram, while complex and based on several educated assumptions about the protolith, temperatures, and waters, demonstrates that ultra-low-$\delta^{18}O$, δD Paleoproterozoic protolith was affected by heavier $\delta^{18}O$ waters. Any secondary high-T exchange with any types of subsequent external waters will result in elevated δD values in biotites and amphiboles and also yield slightly higher than equilibrium $\delta^{18}O$ values of micas, noticeable in some crystal clusters on Fig. 1. However, either of these secondary fluids, or their time-integrated combination cannot explain large range of whole-rock $\delta^{18}O$ values, which reflect the primary value of heterogeneous, hydrothermally-altered protolith.

Isotopic fractionations used:

Graham, C.M.; Harmon, R.S.; and Sheppard, S.M.F. (1984) Experimental hydrogen isotope studies: Hydrogen isotope exchange between amphibole and water; Amer. Mineral. 69, 128-138.

Savin, S.M.; and Epstein, S. (1970) The oxygen and hydrogen isotope geochemistry of clay minerals; Geochim. Cosmochim. Acta 34, 43-63

Suzuoki, T.; and Epstein, S. (1976) Hydrogen isotope fractionation between OH-bearing minerals and water; Geochim. Cosmochim Acta 40, 1229-1240.

Zheng, Y.F. (1993) Calculation of oxygen isotope fractionation in hydroxyl-bearing silicates; Earth. Plan. Sci. Lett. 120, 247-263.

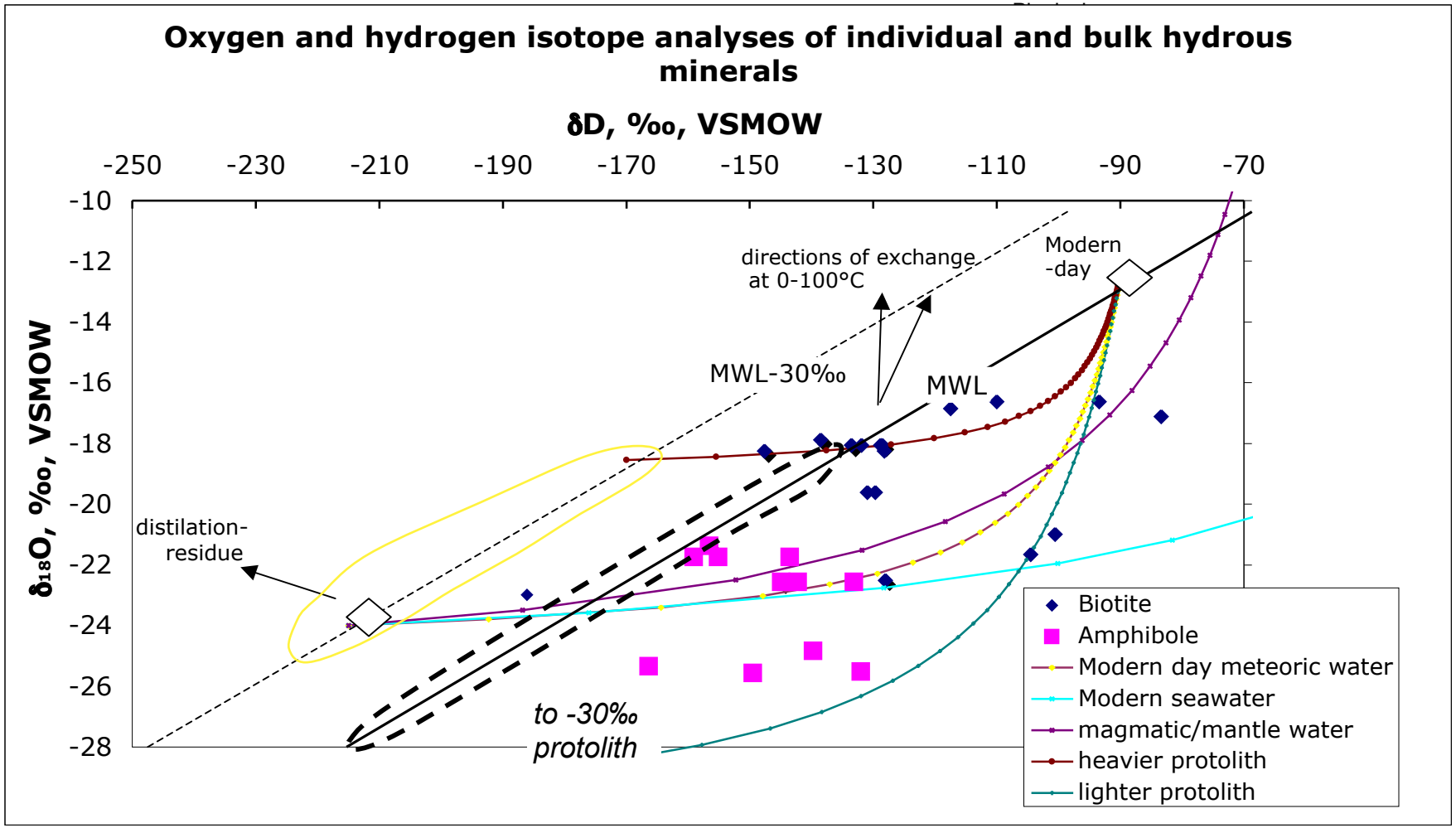

Appendix, Fig. DR1

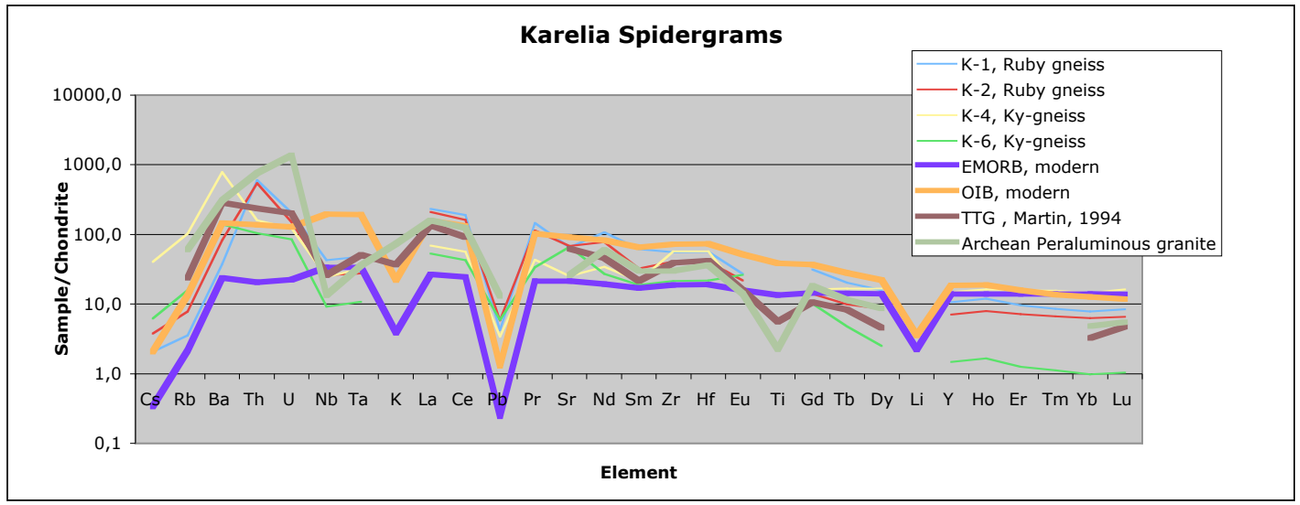

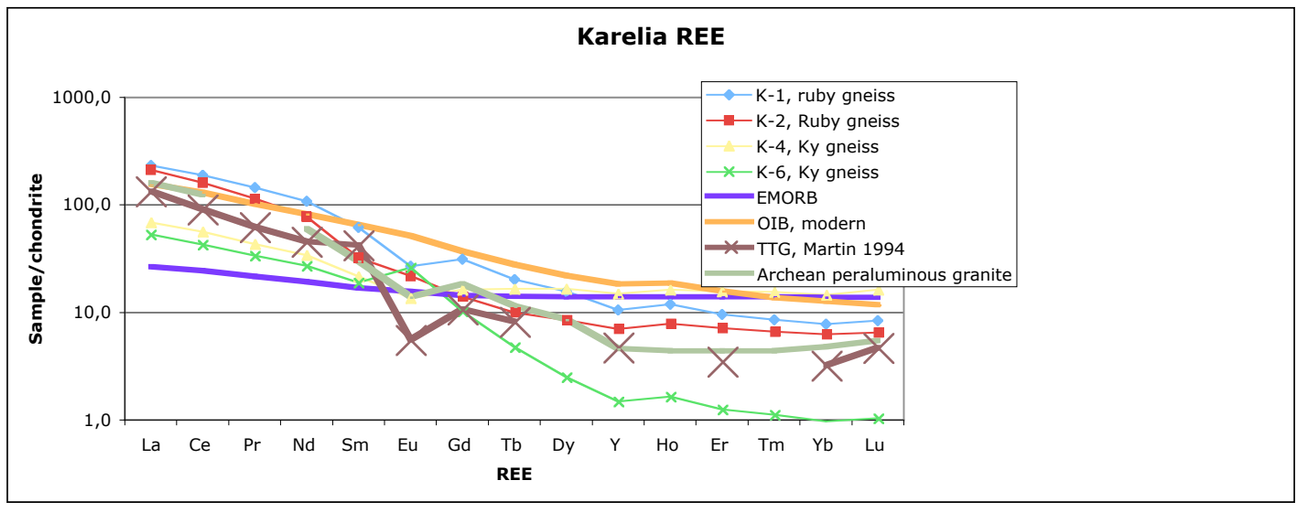

Fig. DR2 Major and trace element analyses of investigated corundum and kyanite plagiogneisses. Figure demonstrates normalized trace elemental pattern as compared to Archean rocks and modern MORB and OIB basalts showing their intermediate to metabasaltic (metagreywacke) composition. The fractionated REE pattern is most consistent with other Archean rock types and derivation within a rift. TTG suites and Archean peraluminous granites are from H. Martin, 1994, The Archean grey gneisses and the genesis of continental crust. in Condie KC Ed Archean crustal evolution, Developments in Precambrian Geology11, Elsevier, pp. 205-260.

Fig. DR3 Field and outcrop photographs
a) Khitostrov outcrop; b) trench across ruby and kyanite-bearing gneisses, c) ruby-bearing plagiogneiss

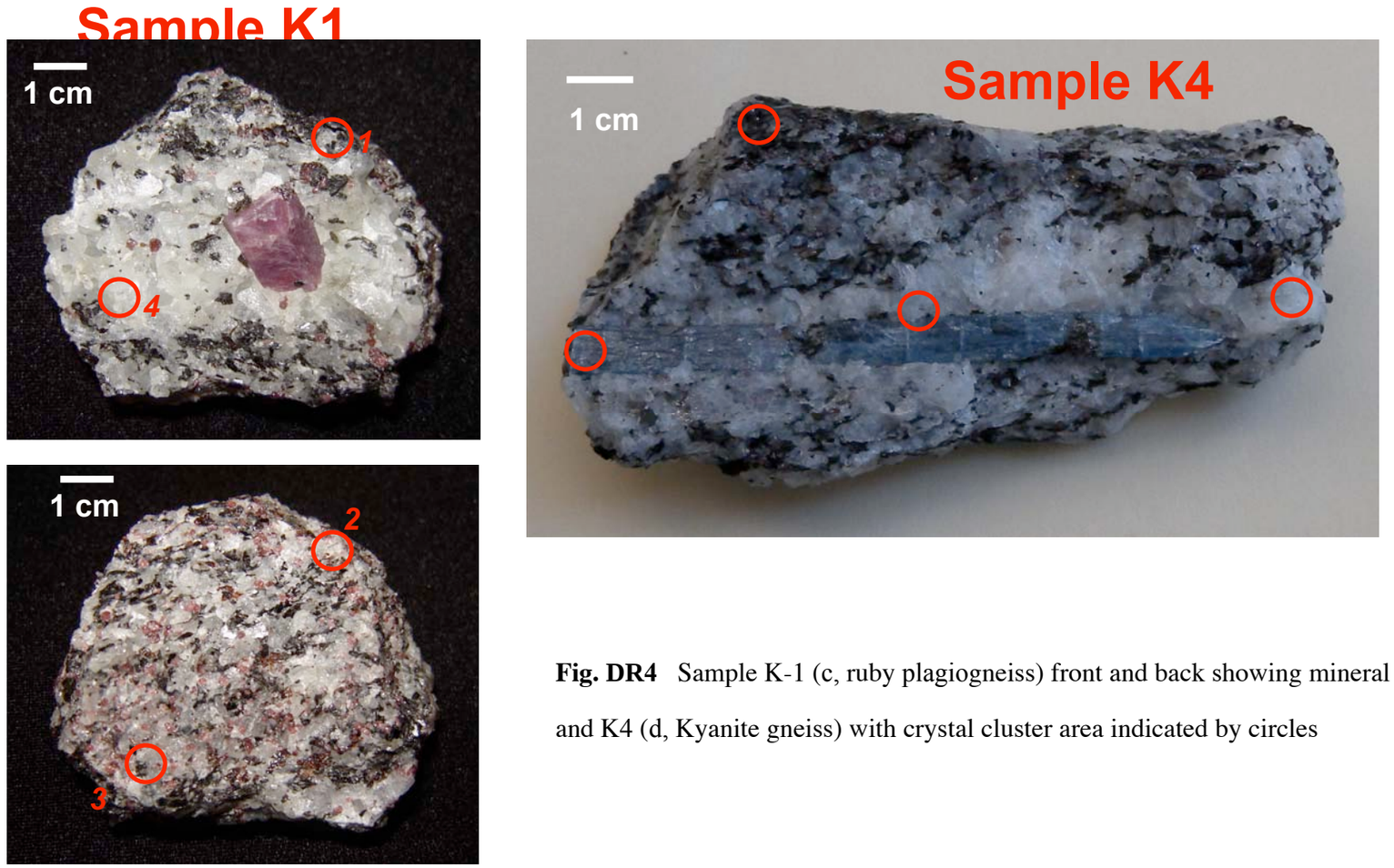

Fig. DR4 Sample K-1 (c, ruby plagiogneiss) front and back showing mineral cluster areas and K4 (d, Kyanite gneiss) with crystal cluster area indicated by circles